JOURNAL OF PROPULSION AND POWER
Vol. 27, No. 1, January–February 2011

Conjugate Design/Analysis Procedure for Film-Cooled Turbine Airfoil Sections

Roger L. Davis*
University of California, Davis, Davis, California 95616
John F. Dannenhoffer III†
Syracuse University, Syracuse, New York 13244
and
John P. Clark‡
U.S. Air Force Research Laboratory, Wright-Patterson Air Force Base, Ohio 45433

DOI: 10.2514/1.48451

An automated procedure is presented for the conjugate Navier–Stokes with heat conduction design and analysis of film-cooled turbine airfoil sections. In this procedure, the internal-cooling plenums inside of the airfoil and the layer of thermal barrier coating are automatically constructed and computational grids for the main flowpath, cooling plenums, turbine walls, thermal barrier coating, and cooling tubes are generated. Embedded overlaid grids are used for the cooling tubes, allowing for any arbitrary placement without regridding of the main flowpath, turbine walls, or cooling plenums. The multidisciplinary use of embedded overlaid grids makes this approach unique and effective for automated optimization procedures. The techniques used to construct the geometry and various computational grids and the treatment of embedded overlaid grids in the Navier–Stokes procedure are described. Demonstration of the procedure is provided for a transonic turbine vane.

Nomenclature

c_p	=	specific heat at constant pressure
k	=	thermal conductivity or turbulent kinetic energy
Pr	=	Prandtl number
T	=	temperature
t	=	time
V	=	velocity magnitude
V_{ol}	=	cell volume
x	=	axial Cartesian direction
y	=	tangential Cartesian direction
Δl_i	=	spacing across computational cell in i direction
Δn	=	spacing normal to fluid/wall interface
μ	=	molecular viscosity

Subscripts

c	=	cooling
f	=	fluid
s	=	solid
w	=	wall
∞	=	freestream

I. Introduction

DESIGN and analysis of film-cooled turbine blades is a complex task involving not only the thermal analysis of the airfoil metal and coatings, but also the fluid dynamic analysis of the cooling-flow effects on the outer surface heat transfer and aerodynamics. The mass, momentum, and thermal effects of the cooling flows were first modeled as surface transpiration source terms in main flowpath Navier–Stokes simulations by Dorney and Davis [1,2]. This approach allowed for efficient optimization of the cooling-hole locations, blowing ratios, and injection angles in two-dimensional airfoil section analysis or three-dimensional airfoil design. It did not, however, provide any thermal information regarding the airfoil metal or the interaction between the airfoil metal and internal, external, or cooling-tube flowfields. Details of the mixing between the cooling and main flowpath flows were also absent.

Much research has been ongoing over the past several decades related to turbine film-cooling using flowfield analysis without solving the heat conduction in the airfoil material. Navier–Stokes analyses of the interaction between the cooling flow and main flowpath were attempted as early as 1978 using parabolized numerical techniques [3]. Since then, time-marching Navier–Stokes analyses have been increasingly used to analyze the interaction between the cooling flow and main flowpath, focusing on issues related to proper grid resolution [4–8], turbulence modeling [9–11], and accurate prediction of cooling effectiveness [12,13]. Several other research efforts have focused on predicting the mixing-flow physics between the injected cooling air and the freestream that are due to cooling-hole shape [14,15] and entrance effects [16]. Dawes et al. [17] developed a 3-D automated unstructured-grid generation procedure using an octree-based cut-Cartesian method with a level-set geometry representation. Heidmann et al. [18] investigated the three-dimensional heat transfer of a turbine vane, including the cooling plenums, cooling holes, and external flowpath. A multiblock structured computational grid was used for all regions of the flow in conjunction with a fixed wall temperature boundary condition. The disadvantage of these types of flow analyses for heat transfer prediction lies in the requirement of either a prescribed surface temperature or heat flux distribution, which is usually unknown to sufficient detail.

Recent advances have been made in coupling flowfield analysis with heat conduction analysis for the airfoil materials in conjugate heat transfer simulations. Several of these efforts have focused on comparison between traditional heat transfer with conjugate analyses [19] and the effect of turbulence modeling [20] and geometry [21–23] on the heat transfer of film-cooled turbines. In several other efforts, progress has been made in automating the arduous task of

Presented as Paper 2009-1461 at the 48th AIAA Aerospace Sciences Meeting, Orlando, FL, 4–7 January 2009; received 7 December 2009; revision received 1 August 2010; accepted for publication 3 September 2010.

*Professor, Mechanical and Aerospace Engineering; davisrl@ucdavis.edu. Associate Fellow AIAA.
†Associate Professor, Mechanical and Aerospace Engineering; jfdannen@syr.edu. Associate Fellow AIAA.
‡Turbine Branch; john.clark3@wpafb.af.mil. Associate Fellow AIAA.

model construction and grid generation. Dawes et al. [24] recently extended their octree-based unstructured-grid approach for conjugate simulations in film-cooled turbines. Goormans-Francke et al. [25] developed a semi-automated multiblock structured-grid approach for film-cooled turbine conjugate heat transfer simulations. Yamane and Yamamoto [26] demonstrated the possibility of using multiblock overlaid structured grids for these types of conjugate simulations.

In the current effort, an automated approach for designing and analyzing the aerothermal fields of a two-dimensional film-cooled turbine airfoil section is described and demonstrated. The purpose of this procedure is to provide designers with a single tool to optimize turbine metal temperature distributions, cooling effectiveness, and aerodynamic performance early in the design cycle. The procedure consists of a technique to generate a multiplenum internal-cooling geometry for a specified airfoil shape and automatically creates the computational grid in both the solid and fluid domains. Overlaid grids are used for the film-cooling tubes to allow cooling air to pass from the internal plenums, through the solid, and into the main flowpath. This provides a unique first-time demonstration of overlaid grids in conjunction with multiblock point-matched grids for a multidisciplinary simulation. A similar approach was recently suggested by Yamane and Yamamoto [26], but multidisciplinary overlaid grids and realistic turbine applications were absent in their investigation. The time-averaged unsteady solutions for the solid and flowfields are provided using parallel procedures targeted for a desk-side cluster of CPUs/cores or combined CPUs/GPUs (graphical processing units). Time-averaged unsteady detached-eddy simulations are preformed for the turbulent flow to provide the effects of self-excited unsteadiness on aerothermal performance. These numerical techniques are described and the procedure is demonstrated for a turbine vane with conditions similar to those found in an advanced low-bypass turbofan engine.

II. Geometry/Grid Generation Procedure

The MBFLO [20] two-dimensional Navier–Stokes procedure has been the computational platform used for the current investigation, along with the CASCADE [27] grid generation procedure. The CASCADE procedure generates an OHHH grid for any turbomachinery cascade section, where an O-grid surrounds the airfoil and H-grid blocks are upstream of the leading edge, downstream of the trailing edge, and through the midpassage. Further decomposition of these blocks is automatically performed to enable parallel computing and fast turnaround of Navier–Stokes solutions. Figure 1a shows an outline of the OHHH grid blocks, and Fig. 1b shows the resulting grid decomposition for a transonic turbine vane.

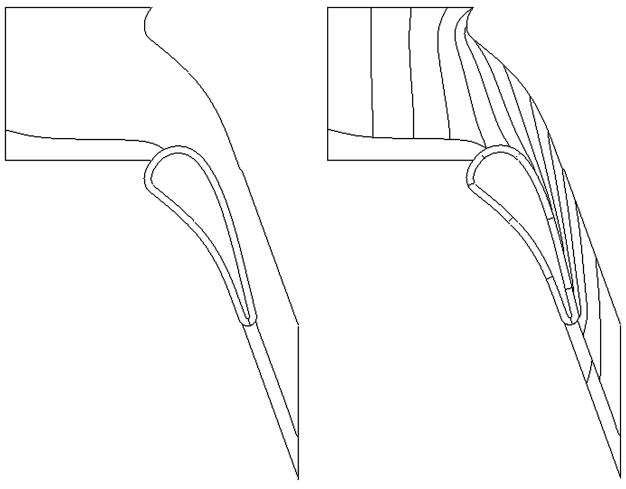

a) OHHH grid blocks **b) Decomposed grid blocks**

Fig. 1 Turbine vane main flowpath blocks.

A. Cascade Procedure

During the current investigation, the CASCADE grid generator was extended to automatically construct cooling plenums, metal walls, thermal barrier coatings (TBCs), and cooling tubes based on additional prescribed design information. This information included the number of interplenum walls, the airfoil wall and TBC thicknesses, the number of cooling tubes, and the trailing-edge strategy (plenum or solid). For each interplenum wall, the axial coordinate of the intersection points with the upper and lower surfaces of the airfoil are prescribed, along with the interplenum wall thickness. In addition, the total pressure and total temperature incoming to that plenum is prescribed (to be discussed further below). For each cooling tube, the axial coordinate at which the cooling tube exits into the main flowpath and at which (upper or lower) side the cooling tube exits are prescribed, along with the cooling-tube diameter and angle. The cooling-tube angle can be referenced either to the absolute positive horizontal or relative to the surface tangent at the injection site. The automated construction of the cooling plenums, wall, thermal barrier coating, and film-cooling tubes will now be discussed.

B. Automated Cooling Plenum, Wall, TBC, and Tube Construction

Generation of the cooling plenums, wall and TBC surfaces, and cooling tubes is performed in eight steps:

1) Create the inner and outer boundaries of the thermal barrier coating, if it exists. The TBC thickness may be added to or subtracted from the specified airfoil coordinates normal to the surface depending on if the specified TBC thickness is positive or negative. Since the TBC is usually very thin relative to the metal wall thickness, the creation of the appropriate (inner or outer) TBC boundary is straightforward.

2) Locate the nearest computational point in the main flowpath O-grid to the prescribed upper and lower interplenum points. This step essentially divides the area inside of the airfoil into plenum domains.

3) Determine how many computational points will exist along each interplenum wall. This is determined from the average grid spacing on the airfoil main flowpath surface used in the O-grid and the length of any given interplenum wall. Points are evenly distributed along each interplenum wall. As a result of this step, each plenum wall has an associated outer discretized boundary.

4) Determine the locus of points that defines the wall inner boundary (see Fig. 2). Initially, one may take the strategy of identifying the inner wall boundary by simply projecting the surface normal by the prescribed airfoil wall thickness. This strategy works well for thin-airfoil wall thicknesses but is not acceptable for nominal wall thicknesses, where overlapping occurs in the leading- and trailing-edge regions, due to high curvature. To avoid this problem and make the technique robust, a different approach must be taken. In the current scheme, the inner wall boundary is found by scaling the plenum wall outer boundary about the centroid of the plenum outer wall. This guarantees a nonoverlapping wall mesh. The scaling factor

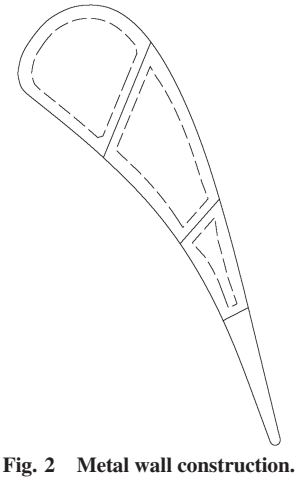

Fig. 2 Metal wall construction.

is determined from an iterative procedure in which the difference between the average normal distance between inner and outer walls and the desired airfoil wall thickness is driven to zero. The result of step 4 leads to the desired average airfoil wall thickness, but does not guarantee that the interplenum wall thicknesses are kept at the prescribed values.

5) Correct the interplenum wall thickness by moving the inner wall location along each interplenum wall such that the normal distance is one-half (due to the O-grid topology) of the prescribed interplenum wall thickness. The corner regions of the inner wall can sometimes take on a shape that is not consistent with the outer wall boundary, requiring some smoothing of those regions. The inner boundary of the wall also becomes the outer boundary of the plenum.

6) Construct the inner boundary of the plenum, where the flow enters the plenum, by scaling the outer boundary of the plenum about its centroid (as shown in Fig. 3). Currently, a fixed scale factor of 0.2 is chosen.

7) If a plenum is desired in the trailing-edge region, then use steps 2–5 to create it. However, if a solid trailing-edge region is desired (as shown in Figs. 2 and 3), then the outer wall of that region is defined from the interplenum wall closest to the trailing edge and the points in the main flowpath along the outer surface of the airfoil.

8) Generate cooling tubes from a fixed generic domain that is scaled, translated, and rotated appropriately before their placement to the desired regions. As stated above, the strategy for the cooling tubes is to use overlaid grids, thereby allowing for arbitrary placement. The generic domain starts with a 1×1 unit model. The length of any given cooling tube can be determined from a distance that traverses along the particular cooling-tube angle from an appropriate point into the main flowpath O-grid to an appropriate point into the desired plenum grid. The height of the cooling tube is scaled to be the prescribed effective cooling-tube diameter. Cooling tubes are then placed at the prescribed locations (see Fig. 4). Upon completing this step, the computational grids in all regions can be generated. Note that by constructing the cooling tubes in this fashion, they may be modified, added, or subtracted easily without affecting the remainder of the blocks/grids.

C. Automated Grid Generation

The computational grids inside of the airfoil are algebraically generated initially and then smoothed using a Poisson smoothing algorithm [28,29]. An O-grid topology is used for the plenums and walls, with the exception of an optional trailing-edge solid wall grid, where an H-grid topology is used. Figure 5a shows examples of the O-grids used for the plenums and walls, and Fig. 5b shows an example H-grid used for a solid trailing-edge wall. The O-grid topology used in the plenum allows the grid to be clustered near the wall and provides accuracy and stability for the turbulence model.

The computational grid for the TBC consists of an O-grid around the airfoil that is similar to the main flowpath O-grid. The TBC

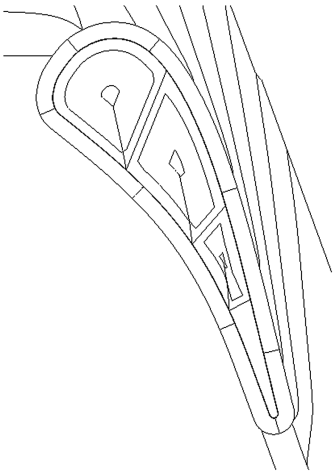

Fig. 3 Plenum construction.

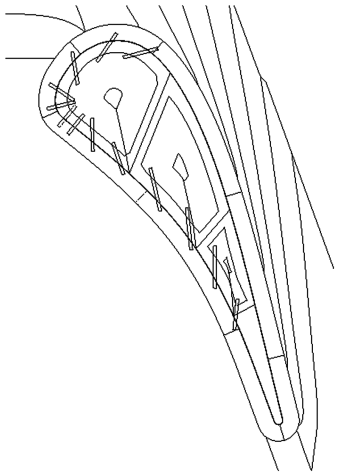

Fig. 4 Cooling-tube construction.

O-grid is subsequently subdivided in the streamwise direction, just as with the main flowpath grid, to reduce memory requirements. The wall and TBC grids are uniformly spaced normal to the wall boundaries.

The computational grids used for the cooling tubes have an H-grid topology in which the grid is stretched from each cooling-tube wall to the centerline of the cooling tube. Figure 6 demonstrates how the cooling-tube grids are placed to connect the internal plenums with the main flowpath. As mentioned above, the placement of the cooling tubes is currently controlled by the user, but could just as easily be performed using an automated design optimization procedure.

Details of the original grid generation of the main flowpath and subsequent decomposition are described in [27]. The resulting overall computational grid produced from the extended CASCADE procedure for the example turbine is shown in Fig. 7.

III. Flow Solution Procedure

The unsteady Favre-averaged governing flowfield equations for an ideal compressible gas in the right-handed Cartesian coordinate system using relative-frame primary variables are used in the MBFLO code. Additional governing equations are also solved, as developed by Wilcox [30–32] for the transport of turbulent kinetic energy and turbulence dissipation frequency in regions of the flow where the computational grid or global time-step size cannot resolve the turbulent eddies. In regions of the flow where the larger-scale eddies can be resolved with the computational grid, techniques borrowed from large-eddy simulation are used to represent the viscous shear and turbulent viscosity. The large-eddy subgrid model described by Smagorinsky [33] is modified according to the detached-eddy considerations described by Strelets [34] and Bush

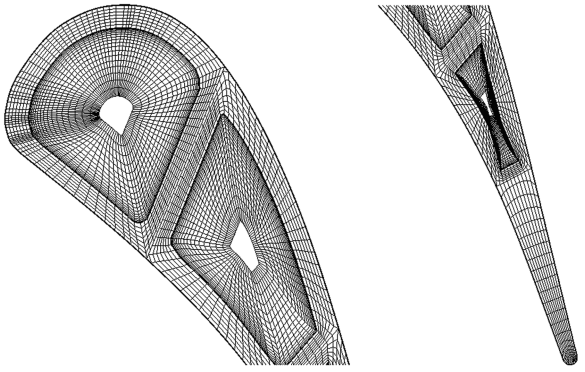

a) Plenum and wall O-grids **b) Traling-edge wall H-grid**

Fig. 5 Grids used internal to the turbine airfoil (every other grid point shown in each direction).

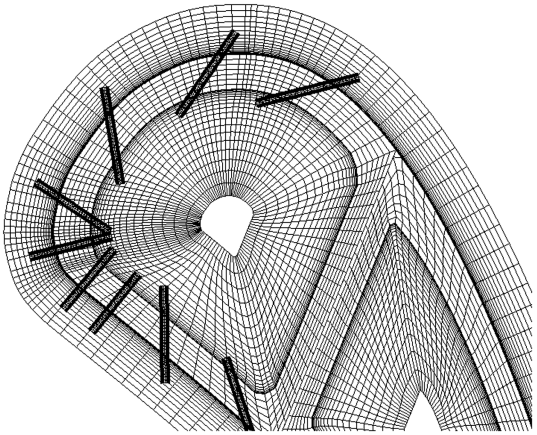

Fig. 6 Embedded overlaid grids used for cooling with internal and main flowpath O-grid (every other grid point shown in each direction).

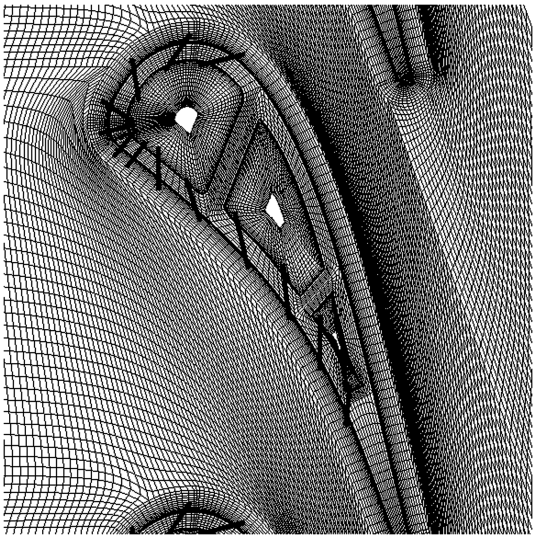

Fig. 7 Overall conjugate grid (every other grid point shown in each direction).

and Mani [35]. In this model, the turbulent viscosity is determined with

$$\mu_t = \rho l_{le} \sqrt{k} \tag{1}$$

where l_{le} is an eddy length scale, proportional to the grid/time-step filter width Δ:

$$l_{le} = \min\left(\frac{\sqrt{k}}{\omega}, \beta^* C_{\text{des}} \Delta\right) \tag{2}$$

and

$$\Delta = \max(\Delta l_i, \sqrt{k}\Delta t, V\Delta t) \tag{3}$$

In addition, the dissipation term $\beta^* \rho k \omega$ of the Wilcox [30–32] turbulent kinetic energy transport equation is limited by the eddy length scale l_{le}, according to

$$\beta^* \rho k \omega \Rightarrow \beta^* \rho k \max\left(\omega, \frac{\sqrt{k}}{\beta^* C_{\text{des}} \Delta}\right) \tag{4}$$

where C_{des} is a proportionality coefficient with a value of 0.65.

The mass, momentum (Navier–Stokes), and energy conservation equations are solved using a Lax–Wendroff control-volume time-marching scheme as developed by Ni [36], Dannenhoffer [37], and Davis et al. [38,39]. Numerical solution of unsteady flows can be performed with either the explicit [36] or a dual-time-step procedure [40]. These techniques are second-order-accurate in time and space. A multiple-grid convergence acceleration scheme [36] is used for steady Reynolds-averaged solutions and the inner convergence loop of unsteady simulations using the dual-time-step scheme. MBFLO has 2-D [27] (shown here), axisymmetric [41] (with and without swirl), and 3-D [42] versions.

Parallel versions of the MBFLO suite of codes exist in addition to the serial versions. Parallelization is performed using the message-passing interface (MPI) library [43] for CPU/core clusters or using both MPI and CUDA[§] libraries for CPU/GPU clusters. Parallel efficiency using MPI on CPU/core clusters has been benchmarked [27] at 85%. Speedups from 7 to 10.5 have been benchmarked [44,45] on CPU/GPU clusters over an equivalent number of CPUs/cores.

The MBFLO2 code has been extended to compute overlaid blocks and point-matched blocks for either fluid or solid domains. This provides a unique capability that significantly increases the flexibility to model complex configurations without the need to spend large resources for grid generation. Figure 8 shows a flowchart of the original (point-matched) solution procedure in solid-line boxes, with the additional kernels to handle fluid or solid overlaid blocks shown in dashed-line boxes. Any combination of overlaid grids can be handled, including fluid blocks overlaid onto fluid or solid blocks and solid blocks overlaid onto fluid or solid blocks.

A. Flow Treatment in Cooling Tubes

The cooling-tube blocks are overlaid onto both fluid and solid blocks, as shown in Fig. 6. The cooling-tube blocks are a unique application of overlaid grids, in that the values of the primary variables and their changes at all points along all edges are interpolated from the underlying fluid and solid blocks as boundary conditions. These blocks also have greater local grid densities than their underlying blocks. As such, the solutions in these blocks are considered to be superior to that of the points in the underlying blocks contained within the boundaries of the cooling-tube blocks. Thus, the cooling-tube blocks could be considered to be embedded blocks.

In those regions where the cooling-tube blocks are overlaid onto fluid blocks (in the cooling plenums and main flowpath), the flow primary variables at the boundaries and ghost nodes are interpolated from the underlying fluid blocks. In those regions where the cooling-tube blocks are overlaid onto solid blocks (over the wall and TBC), the temperature at the tube block boundaries is interpolated from the underlying solid blocks as an initial step of the conjugate boundary condition treatment (described below).

After the flow equations are integrated in the cooling tubes and physical boundary conditions are applied in all blocks before updating the primary variables, the changes in the flow primary variables are corrected at the boundaries of the cooling-tube blocks. This keeps the cooling-tube boundary primary variables consistent with the underlying block values. In those regions where the fluid cooling-tube blocks are overlaid onto fluid blocks, the changes of the primary variables are interpolated from the underlying fluid blocks. In those regions where the cooling-tube blocks are overlaid onto solid blocks, the conjugate and no-slip boundary conditions, described below, are applied.

B. Treatment of Blocks Underlying Cooling Tubes

As previously mentioned, the cooling-tube blocks have overlaid boundaries on all sides, making them essentially embedded blocks with greater grid densities and a superior solution. As a result, all primary variables in regions of fluid blocks that are overlaid by the cooling-tube fluid blocks are replaced with interpolated values from the cooling-tube blocks. Interpolation of the solution at points in the underlying blocks makes the variables consistent and makes communication between the blocks stronger.

[§]Data available online at http://developer.nvidia.com/object/cuda_training.html [retrieved 2010].

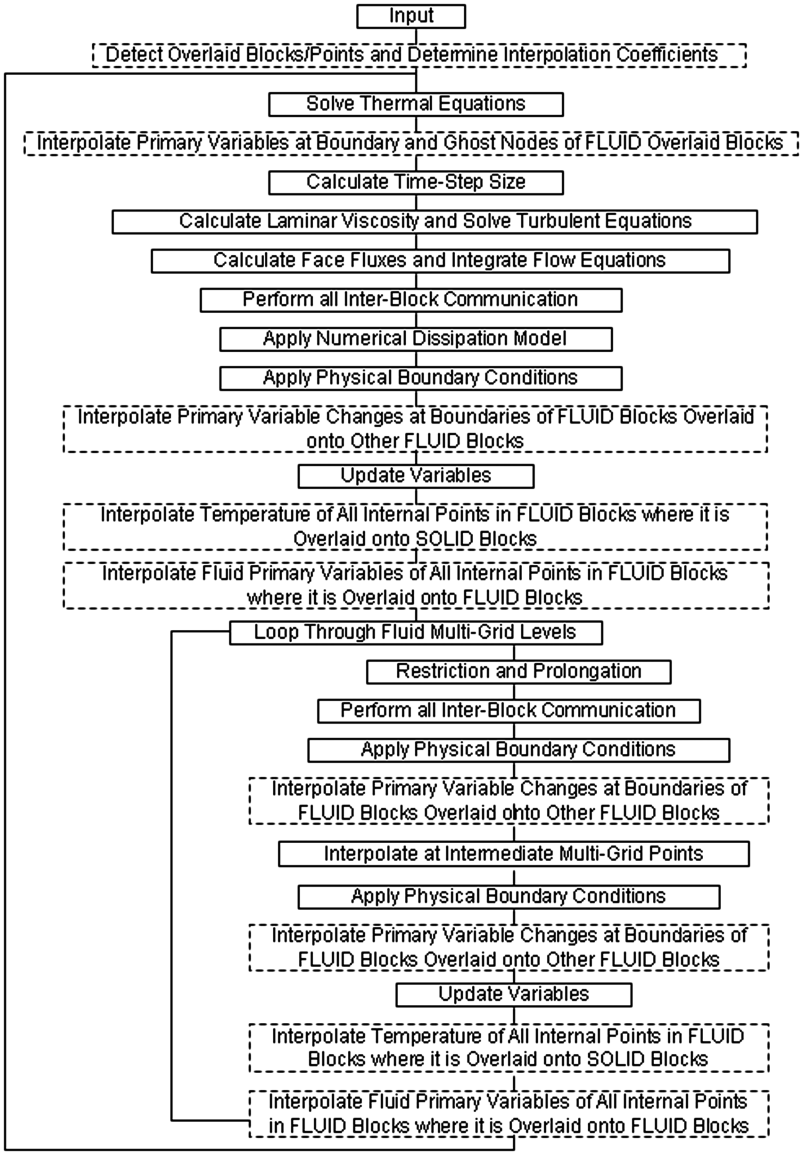

Fig. 8 Flowchart of extended MBFLO procedure.

Similarly, the temperature in regions of solid blocks that are overlaid by the cooling-tube fluid blocks is replaced with the fluid temperature after each update of the fluid variables. The purpose of this treatment is to replace the solid with the fluid in those regions. In essence, the overlaid cooling-tube blocks drill holes through the solid wall blocks. Again, the advantage of using overlaid grids for this purpose is that the grids can be arbitrarily placed without the need for regridding both the cooling plenums and the main flowpath. Thus, this approach lends itself very well to automated optimization schemes.

C. Overlaid-Grid Interpolation

Before the conjugate solution procedure begins as a preprocessing step, the computational points that lie inside any other block in the domain (either fluid or solid) are identified using an efficient two-level search routine. In the first level, each point in a given grid block is first checked to see if it lies within the bounding box of any other grid block. The block bounding box is defined as the minimum and maximum grid coordinates of the points that lie along the perimeter of the block. If a grid point is determined to be within the block bounding box, then a second-level search is performed through the cells of that block to see if the point lies within the bounding box of the cell. The cell bounding box is simply defined as the minimum and maximum grid coordinates of the four corners that make up the cell. If the point is determined to be within the bounding box of a cell, then the interpolation coefficients of that point are determined using a bilinear shape function.

A list is created that consists of the block number, indices of the point that was found to be in another block, the block number and cell indices in which the point was found, and the i- and j-wise interpolation coefficients. The tolerance for the bounding-box searches is quite small (10^{-8}), since many points could lie in viscous flow regions, where the grid spacing is very small. Without the bounding-box filter, the search would be an N^2 operation for two dimensions and would take considerable time. However, with the block and cell bounding-box filters, the search can be performed in seconds.

During the conjugate time-marching iteration, the interpolation of points that lie inside, on the boundary, or in the ghost nodes of an overlaid grid can be performed very quickly by looping through the list of points. In MBFLO2, separate interpolation routines are created to make processing even more efficient. These routines are shown as dashed-line boxes in Fig. 8.

D. Boundary Conditions

Conjugate boundary conditions are applied at all interfaces between fluid and solid blocks, as described below. At the inlet to the cooling plenums, the total pressure and total temperature are held at

prescribed values. The flow angle is held normal to the cooling plenum boundary pointing inward into the plenum block. As a result of these boundary conditions, the mass-flow rates of the cooling tubes are predicted rather than prescribed. The boundary conditions used in the main flowpath are those typically used in turbomachinery simulations; the total pressure, total temperature, and flow angle are held at the inlet and the static pressure is held at the exit.

IV. Thermal Solution Procedure

In solid blocks, the solution to the transient heat conduction equation, given in Eq. (5), is performed using a finite volume method [46] similar to that used for the flow equations:

$$\rho_s \cdot c_{p_s} \frac{\partial T_s}{\partial t} = k_s \cdot \left[\frac{\partial^2 T_s}{\partial x^2} + \frac{\partial^2 T_s}{\partial y^2} \right] \tag{5}$$

The heat conduction equation is integrated around the primary mesh cell to obtain spatial first derivatives of the temperature at the cell centers. This step is followed with a second integration around secondary mesh cells made by connecting the cell centers surrounding any given node to obtain the spatial second derivatives of the temperature. For unsteady Reynolds-averaged Navier–Stokes (RANS) or detached-eddy simulations, a dual-time-step approach [40] is used that is second-order-accurate in both space and time. A gather–add operation is used to distribute second derivatives to appropriate nodal points in the grid. This technique eliminates the need for ghost nodes of temperature and reduces simulation memory needs. For steady-flow simulations and during the inner iteration of the dual-time-step scheme, discretization of Eq. (5) is performed using a simple explicit backward difference in time. The accuracy of this technique is first order in time and second order in space. This method is stable, provided the following condition for simulation time step holds (where CFL is the Courant–Friedrichs–Lewy number):

$$\Delta t_s \leq \frac{\mathrm{CFL} \cdot \rho_s \cdot c_{p_s}}{k_s} \left[\frac{\mathrm{Vol}^2}{\Delta x^2 + \Delta y^2} \right] \tag{6}$$

For fluid blocks adjacent to solid walls, the conjugate no-slip boundary condition is applied. This boundary condition [46] maintains a consistent temperature and heat flux between the solid and fluid interface:

$$T_i = \left(\frac{k_f \cdot T_{fw+1}}{\Delta n_f} + \frac{k_s \cdot T_{sw+1}}{\Delta n_s} \right) \Big/ \left(\frac{k_f}{\Delta n_f} + \frac{k_s}{\Delta n_s} \right) \tag{7}$$

The values of k_s, c_{ps}, and ρ_s are specified for the solid material. The value of k_f is determined from the flow specific heat c_{pf}, local value of molecular viscosity μ, and specified Prandtl number Pr, according to

$$k_f = \frac{c_{p_f} \mu}{Pr} \tag{8}$$

V. Results: Demonstration of Procedure

The conjugate design/analysis procedure is demonstrated using a transonic turbine vane tested experimentally (uncooled) by Arts et al. [47], for which the airfoil/cascade geometry is available and the computational blocks and grid are shown in Figs. 1–7. The geometry and flow conditions for the simulations shown below are listed in Table 1. The grid shown in these figures consists of 52 blocks (27 fluid blocks, 12 solid blocks, and 13 overlaid cooling-tube fluid

Table 1 Geometry and flow conditions of a transonic turbine

Parameters	Values	Parameters	Values
Geometry		*Turbine metal conditions*	
Interplenum wall thickness	0.02444 cm (0.096 in.)	Wall thickness	0.0209 cm (0.072 in.)
Cooling-tube diameter	0.00488 cm (0.0192 in.)	Initial metal temperature	763.3 K (1374 R)
Airfoil axial chord	3.698 cm (1.456 in.)	Thermal conductivity	15 W/(mK) (1.8735 lbf/(s R))
Cascade pitch	5.75 cm (2.2638 in.)	Specific heat	480 J/(kg K) (2870.55 ft^2/(s^2 R))
Main flowpath conditions		Density	8000 kg/m^3 (15.52 slugs/ft^3)
Inlet total pressure	2096 kPa (43,776 psf)	*TBC conditions*	
Inlet total temperature	1680.6 K (3025 R)	TBC thickness	0.0061 cm (0.024 in.)
Inlet Mach number	0.15	Initial metal temperature	763.3 K (1374 R)
Exit isentropic Mach number	0.875	Thermal conductivity	0.12 W/(mK) (0.015 lbf/(s R))
Inlet angle (from horizontal)	0	Specific heat	1090 J/(kg K) (6518.54 ft^2/(s^2 R))
Exit static pressure	1308.6 kPa (27,330 psf)	Density	1420 kg/m^3 (2.7548 slugs/ft^3)
Inlet axial chord Reynolds number	337,711.00	*Plenum 1 conditions*	
Prandtl number	0.685	Inlet total pressure	2178.7 kPa (45,504 psf)
Turbulent Prandtl number	0.95	Inlet total temperature	818.9 K (1474 R)
Inlet turbulence intensity	6.00%	*Plenum 2 conditions*	
Inlet dissipation length scale	0.00093 m (0.003064 ft)	Inlet total pressure	2178.7 kPa (45,504 psf)
Ratio of specific heats	1.3	Inlet total temperature	791.1 K (1424 R)
Pressure-side cooling holes [a]		*Plenum 3 conditions*	
Hole-1 axial location	0.0152 cm (0.006 in.)	Inlet total pressure	2178.7 kPa (45,504 psf)
Hole-1 relative angle to local tangent	90	Inlet total temperature	763.3 K (1374 R)
Hole-2 axial location	.1524 cm (0.06 in.)	*Suction-side cooling holes*[a]	
Hole-2 relative angle to local tangent	90	Hole-1 axial location	0.03048 cm (0.012 in.)
Hole-3 axial location	0.3048 cm (0.12 in.)	Hole-1 relative angle to local tangent	70
Hole-3 relative angle to local tangent	90	Hole-2 axial location	0.3048 cm (0.12 in.)
Hole-4 axial location	0.6096 cm (0.24 in.)	Hole-2 relative angle to local tangent	50
Hole-4 relative angle to local tangent	50	Hole-3 axial location	0.9144 cm (0.36 in.)
Hole-5 axial location	1.0668 cm (0.42 in.)	Hole-3 relative angle to local tangent	50
Hole-5 relative angle to local tangent	30	Hole-4 axial location	1.524 cm (0.6 in.)
Hole-6 axial location	1.6764 cm (0.66 in.)	Hole-4 relative angle to local tangent	50
Hole-6 relative angle to local tangent	30	*Plenum wall intersection locations*[a]	
Hole-7 axial location	2.1956 cm (0.864 in.)	Wall-1 suction side	1.8288 cm (0.72 in.)
Hole-7 relative angle to local tangent	30	Wall-1 pressure side	1.2192 cm (0.48 in.)
Hole-8 axial location	2.5908 cm (1.02 in.)	Wall-2 suction side	2.8194 cm (1.11 in.)
Hole-8 relative angle to local tangent	30	Wall-2 pressure side	2.286 cm (0.9 in.)
Hole-9 axial location	2.9261 cm (1.152 in.)	Wall-3 suction side	3.2614 cm (1.284 in.)
Hole-9 relative angle to local tangent	30	Wall-3 pressure side	2.8956 cm (1.14 in.)

[a]Measured from the leading edge.

Table 2 Predicted cooling-flow statistics of time-averaged DES solution[a]

	Blowing (mass-flow) ratio	Area-averaged velocity ratio	Area-averaged temperature ratio
		Pressure side (from leading edge)	
Hole-1	0.011	0.846	0.459
Hole-2	0.008	0.598	0.512
Hole-3	0.014	1.065	0.451
Hole-4	0.008	0.544	0.462
Hole-5	0.009	0.630	0.467
Hole-6	0.010	0.738	0.474
Hole-7	0.011	0.793	0.474
Hole-8	0.009	0.704	0.489
Hole-9	0.013	1.057	0.486
		Suction side (from leading edge)	
Hole-1	0.003	0.362	0.681
Hole-2	0.009	0.723	0.462
Hole-3	0.019	1.444	0.450
Hole-4	0.019	1.478	0.456

[a]Main flowpath mass-flow rate is 11.88 kg/s (0.814 slugs/s), velocity is 118.58 m/s (389.04 ft/s), and temperature is 1674.9 K (3014.83 R).

blocks) and 123,014 points. Inflow thermal conditions were prescribed at actual engine conditions, however, as described below, to better demonstrate the capability of the current procedure.

Validation of this conjugate film-cooling capability is difficult due to the lack of experimental data for a real configuration. Simulations have been performed here using realistic geometry and flow conditions in hopes of providing benchmark results for comparison. The flow conditions for the simulations shown here are consistent with those reported for an advanced low-bypass turbofan engine [48]. The turbine airfoil was modeled as steel with an initial temperature of 763.3 K (1374 R), which is similar to the compressor exit total temperature of 818.9 K (1474 R). The main flowpath inlet total temperature was 1680 K (3025 R) and the inlet total pressure was 2096 kPa (43,776 psf), which is the combustor exit temperature. The cooling plenum inlet total pressures and total temperatures given in Table 1 are similar to the compressor exit conditions. In the current simulations, values of the steel and TBC thermal conductivity, specific heat, and density were assumed to be constant, for simplicity. However, these variables could be made functions of local temperature for general simulations, to improve accuracy. As previously described, the thermal conductivity of air was computed from the local coefficient of viscosity, a constant Prandtl number, and the specific heat. The specific heat was determined from specified values of the ratio of specific heats and real gas constant for air. Again, the ratio of specific heats for air could also be made a function of the local temperature, to further improve accuracy.

The design/analysis procedure being developed uses time-averaged detached-eddy simulation (DES), rather than traditional RANS, to include the effects of self-excited unsteady flows on aerothermal performance. This strategy is important to improve prediction accuracy and optimization for modern highly loaded film-cooled airfoils. During any simulation, steady RANS results are initially obtained, immediately followed by an appropriate number of DES time steps to establish the correct aerothermal transients, and finalized by the time-averaging of the flowfield over an appropriate number of time steps. This entire process can be executed in approximately 6 h of clock time using 32 CPUs/cores (3 GHz) in parallel for the application shown below. Although the current simulations have not yet been performed on a CPU/GPU cluster, it is estimated that the turnaround time for this procedure would take approximately 50 min using 32 combined CPUs/GPUs based on the benchmarks [44] that showed a speedup factor of 7 over an equivalent number of CPUs. The steady RANS part of the solution was executed in approximately 90 min of clock time using 32 CPUs/cores (3 GHz) in parallel. The detached-eddy simulations were performed using the implicit dual-time-step procedure with a time-step size of 2.4×10^{-7} s. This time-step size was chosen in order to resolve any self-excited effects due to trailing-edge shedding. Approximately 100 time steps were performed for each trailing-edge shedding cycle. As a result, the unsteady simulations were run for a total of 8000 time steps, which corresponded to approximately 80 trailing-edge shedding cycles. The flow was time-averaged over the final 4000 time steps, or approximately 40 shedding cycles. The predicted time-averaged mass-flow, area-averaged exit velocity, and area-averaged exit temperature of each cooling tube as a percentage of the main flowpath values are given in Table 2.

Figure 9 shows Mach number contours of the steady RANS, instantaneous DES, and time-averaged DES simulations. This figure clearly shows the shedding at the trailing edge in the instantaneous DES results. Comparison of the steady RANS and time-averaged DES results shows that Mach number contours are similar, except in the wake, where the temperature and velocity diffusion is greater, due to the trailing-edge shedding and mixing for the DES.

The temperature contours in the flow and solid domains are shown in Fig. 10. The temperature contours are smooth and continuous across the wall block boundaries, demonstrating that the multiblock solution procedure works properly. The contours in Fig. 10 can be used to quickly see where the temperature of the solid domains is

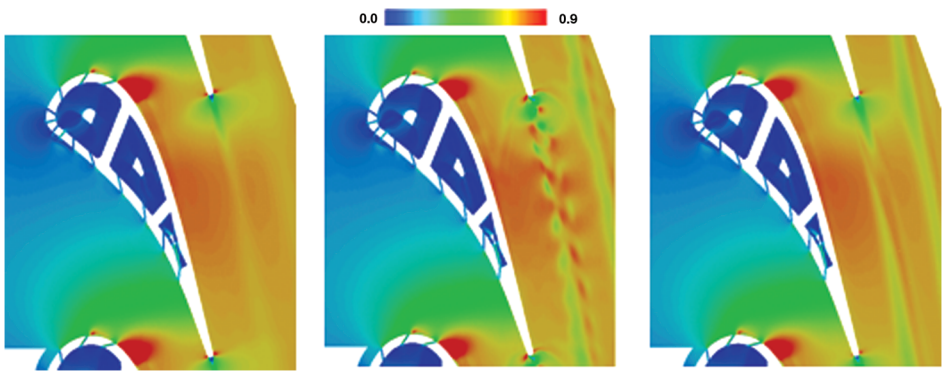

Fig. 9 Mach number contours of flow.

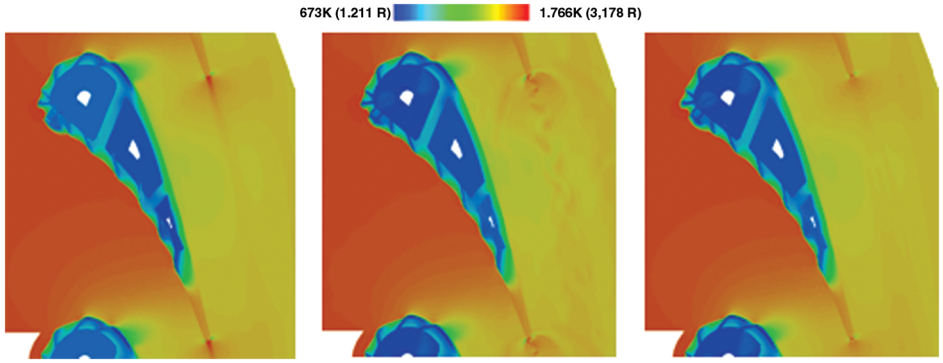

Fig. 10 Temperature contours of flow and solids; the melting temperature of steel is 1670 K (3006 R).

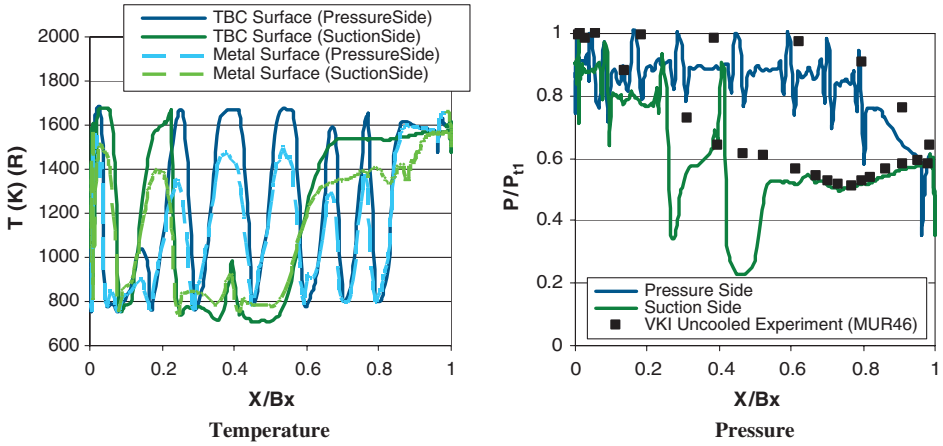

Fig. 11 Temperature and pressure distribution of the vane. VKI is the von Karman Institute for Fluid Dynamics.

high and close to the melting point. For instance, the temperature of the steel in the trailing-edge region is near the melting point in this configuration. As will be demonstrated below, the designer can easily add film-cooling to this region to alleviate this problem. The region of cooling effectiveness of each cooling flow in both the flow and solid domains can also be easily seen in Fig. 10, allowing the designer to either optimize the cooling flow by hand or through an automated optimization procedure [49].

Figure 11 shows the outer surface (main flowpath side) temperature of the thermal barrier coating, the metal (steel) surface temperature (at TBC/metal interface), and the outer surface pressure distribution on the vane from the time-averaged detached-eddy simulation. The temperature distribution shows that the thermal barrier coating has done a good job of isolating the high temperature from the metal. The outer surface temperature of the thermal barrier coating is close or at the melting temperature of the steel in several locations. However, the metal surface temperature is well below this critical temperature throughout the vane. The pressure distribution shows the surface pressure on the outer surface of the thermal barrier coating as well as through the exits of the film-cooling holes. Uncooled experimental data corresponding to the MUR46 test point [47] are shown in this figure as a baseline comparison. The time-averaged detached-eddy pressure distribution has the same trend as the experimental data, but with less loading, due to the additional mass flow from the film-cooling. The jumps in the pressure distribution result from the underexpanded flow from the cooling plenums. The pressure on the suction surface is at the same level as the experimental data; however, the pressure on the pressure surface is lower, due to the additional blockage and greater velocity of the film-cooling flows.

The current two-dimensional procedure can be used to design film-cooled turbine airfoil sections that can be optimized to provide acceptable wall temperature distributions and heat transfer

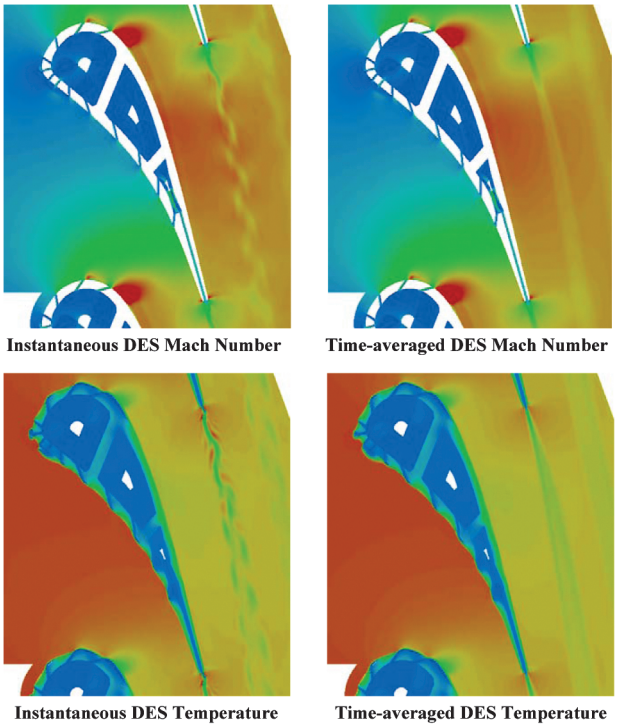

Fig. 12 Effect of adding a cooling tube through the trailing edge (contour variation is the same as those shown in Figs. 9 and 10).

coefficients along with aerodynamic performance. The advantage of the current procedure is the ability to add, modify, or subtract film-cooling tubes without the need for regridding or computing solutions each time from scratch. For instance, the temperature in the trailing edge of the vane, as shown in Fig. 11, is higher than in most other regions of the solid domain. In addition, the unsteady effects due to the trailing-edge shedding shown in Figs. 9 and 10 are quite high. It is well known that trailing-edge blowing can be used to reduce both of these effects. In the current system, it is simple to add another cooling tube through the trailing-edge region exiting at the trailing edge without regenerating and regridding the rest of the domain. Figure 12 shows the results of adding the trailing-edge cooling tube on the instantaneous and time-averaged Mach numbers and temperatures. It is clear through comparison between Figs. 9, 10, and 12 that the trailing-edge blowing has reduced the temperature in the trailing-edge portion of the vane as well as the unsteady shedding downstream of the trailing edge.

VI. Conclusions

A two-dimensional conjugate Navier–Stokes procedure has been developed to automatically generate internal-cooling plenums and cooling tubes based on user-specified parameters and airfoil geometry. Multiblock point-matched structured grids are used everywhere, except for the cooling tubes, where embedded overlaid grids are used to provide maximum flexibility and computational efficiency. Both heat conduction and Navier–Stokes solutions are provided simultaneously for the prediction of the aerothermal fields. A detached-eddy simulation approach is typically used for the flowfield to provide the effects of self-excited unsteadiness. The procedure is targeted for an automated optimization procedure that runs on parallel CPU/core clusters or combined CPU/GPU clusters.

Because of the lack of experimental and simulation results for film-cooled turbine geometry, it is hoped that the current simulation results will serve as a baseline for future comparisons. The current procedure has been demonstrated on a transonic turbine vane for which the geometry is publicly available. Information regarding the flow, metal, TBC, and film-cooling flow characteristics has been provided.

Finally, it is recognized that three-dimensional effects are very important for accurate prediction of turbulence effects with the detached-eddy modeling and of turbulent mixing of the cooling jet flows with the main flowpath. Integration of the current procedure into an automated design optimization procedure and extension to three-dimensional configurations and flows have been considered and are both currently being pursued. Although it was not stated, the current procedure will also be useful in exploring blowing/suction flow-control strategies in the future.

Acknowledgments

The first and third authors would like to thank the managers at the U.S. Air Force Research Laboratory for their support of this effort under contract 09-S590-0009-20-C1. The first author would also like to acknowledge the conjugate development work of Mathew Fife during his M.S. degree program.

References

[1] Dorney, D. J., and Davis, R. L., "Investigation of Hot Streak Migration and Film Cooling Effects on Heat Transfer in Rotor/Stator Interacting Flows," Naval Air Systems Command Rept. N0014-88-C-0677-2, March 1992.

[2] Dorney, D. J., and Davis, R. L., "Numerical Simulation of Turbine 'Hot Spot' Alleviation Using Film Cooling," *Journal of Propulsion and Power*, Vol. 9, No. 3, May–June 1993, pp. 329–336. doi:10.2514/3.23626

[3] Bergeles, G., Gosman, A. D., and Launder, B. E., "The Turbulent Jet in a Cross Stream at Low Injection Rates: A Three-Dimensional Numerical Treatment," *Numerical Heat Transfer*, Vol. 1, No. 2, 1978, pp. 217–242. doi:10.1080/10407787808913373

[4] Leylek, J. H., and Zerkle, R. D., "Discrete-Jet Film Cooling: A Comparison of Computational Results with Experiments," *Journal of Turbomachinery*, Vol. 116, 1994, pp. 358–368. doi:10.1115/1.2929422

[5] Choi, D., "A Navier–Stokes Analysis of Film Cooling in a Turbine Blade," AIAA, Paper 93-158, Jan. 1993.

[6] Weigand, B., and Harasgama, S. P., "Computations of a Film Cooled Turbine Rotor Blade With a Non-Uniform Inlet Temperature Distribution Using a Three-Dimensional Viscous Procedure," American Society of Mechanical Engineers, Paper 94-GT-15, 1994.

[7] Berhe, M. K., and Patankar, S., "A Numerical Study of Discrete-Hole Film Cooling," American Society of Mechanical Engineers, Paper 96-WA/HT-8, 1996.

[8] Walters, D. K., and Leylek, J. H., "A Systematic Computational Methodology Applied to a Three-Dimensional Film-Cooling Flowfield," *Journal of Turbomachinery*, Vol. 119, 1997, pp. 777–785.

[9] Medic, G., and Durbin, P., "Toward Improved Film Cooling Prediction," *Journal of Turbomachinery*, Vol. 124, April 2002, pp. 193–199. doi:10.1115/1.1458021

[10] Guo, X., Schroder, W., and Meinke, M., "Large-Eddy Simulation of Film Cooling Flows," *Computers and Fluids*, Vol. 35, 2006, pp. 587–606. doi:10.1016/j.compfluid.2005.02.007

[11] Tyagi, M., and Acharya, S., "Large Eddy Simulation of Film Cooling Flow from an Inclined Cylindrical Jet," *Journal of Turbomachinery*, Vol. 125, 2003, pp. 734–742. doi:10.1115/1.1625397

[12] Rozati, A., and Tafti, D. K., "Large-Eddy Simulation of Leading Edge Film Cooling: Analysis of Flow Structures, Effectiveness, and Heat Transfer Coefficient," *International Journal of Heat and Fluid Flow*, Vol. 29, 2008, pp. 1–17. doi:10.1016/j.ijheatfluidflow.2007.05.001

[13] Rozati, A., and Tafti, D. K., "Large-Eddy Simulation of Leading Edge Film Cooling—Part II: Heat Transfer and Effect of Blowing Ratio," *Journal of Turbomachinery*, Vol. 130, Oct. 2008, pp. 1–7.

[14] Renze, P., Shroder, W., and Meinke, M., "Hole Shape Comparison for Film Cooling Flows Using Large-Eddy Simulations," AIAA, Paper 2007-907, Jan. 2007.

[15] Lin, C., Holder, R. J., Thornburg, H., Sekar, B., Zelina, J., Anderson, W., Polanka, M. D., Stouffer, S. D., and Briones, A., "Numerical Simulation of Film Cooling in Reactive Flow over a Surface with Shaped Coolant Hole," AIAA, Paper 2009-678, Jan. 2009.

[16] Kohli, A., and Thole, K. A., "A CFD Investigation on the Effect of Entrance Flow Conditions in Discrete Film Cooling Holes," *32nd National Heat Transfer Conference*, Vol. 12, American Society of Mechanical Engineers, New York, 1997, pp. 223–232.

[17] Dawes, W. N., Kellar, W. P., and Harvey, S. A., "Using Level Sets as the Basis for a Scalable, Parallel Geometry Engine and Mesh Generation System," AIAA, Paper 2009-372, Jan. 2009.

[18] Heidmann, J. D., Rigby, D. L., and Ameri, A. A., "A Three-Dimensional Coupled Internal/External Simulation of a Film-Cooled Turbine Vane," *Journal of Turbomachinery*, Vol. 122, April 2000, pp. 348–359. doi:10.1115/1.555450

[19] Starke, C., Janke, E., Hofer, T., and Lengani, D., "Comparison of a Conventional Thermal Analysis of a Turbine Cascade to a Full Conjugate Heat Transfer Computation," American Society of Mechanical Engineers, Paper GT2008-51151, June 2008.

[20] Ledezma, G. A., Laskowski, G. M., and Tolpadi, A. K., "Turbulence Model Assessment for Conjugate Heat Transfer in a High Pressure Turbine Vane Model," American Society of Mechanical Engineers, Paper GT2008-50498, June 2008.

[21] Su, S., Liu, J., Fu, J., Hu, J., and An, B., "Numerical Investigation of Fluid Flow and Heat Transfer in a Turbine Blade with Serpentine Passages and Latticework Cooling," American Society of Mechanical Engineers, Paper GT2008-50392, June 2008.

[22] Rossette, A. H., Mazur, Z., Bautista, E. A., Demeulenaere, A., and Hernandez, J., "Unsteady 3-D Conjugated Heat Transfer Simulation of a Thermal Barrier Coated Gas Turbine Bucket," American Society of Mechanical Engineers, Paper GT2008-50597, June 2008.

[23] Eifel, M., Caspary, V., Honen, H., and Jeschke, P., "Experimental and Numerical Analysis of Gas Turbine Blades with Different Internal Cooling Geometries," American Society of Mechanical Engineers, Paper GT2009-59474, June 2009.

[24] Dawes, W. N., Kellar, W. P., and Harvey, S. A., "Generation of Conjugate Meshes for Complex Geometries for Coupled Multi-Physics Simulations," AIAA, Paper 2010-162, Jan. 2010.

[25] Goormans-Francke, C., Carabin, G., and Hirsch, C., "Mesh Generation for Conjugate Heat Transfer Analysis of a Cooled High Pressure Turbine Stage," American Society of Mechanical Engineers, Paper GT2008-50660, June 2008.

[26] Yamane, T., and Yamamoto, K., "Introduction of Combined Usage of Overset Grid Method in Conjugate Heat Transfer Simulation," American Society of Mechanical Engineers, Paper GT2009-59832, June 2009.
[27] Davis, R. L., and Dannenhoffer, J. F., III, "Detached-Eddy Simulation Procedure Targeted for Design," *Journal of Propulsion and Power*, Vol. 24, No. 6, Nov.–Dec. 2008, pp. 1287–1294. doi:10.2514/1.36680
[28] Sorenson, R. L., "A Computer Program to Generate Two-Dimensional Grids About Airfoils and Other Shaped by the Use of Poisson's Equation," NASA TM-81198, 1980.
[29] Thompson, J. F., Thames, F. C., and Mastin, C. W., "Automatic Numerical Grid Generation of Body-Fitted Curvilinear Coordinate System for Field Containing Any Number of Arbitrary Two-Dimensional Bodies," *Journal of Computational Physics*, Vol. 15, No. 3, July 1974, pp. 299–319. doi:10.1016/0021-9991(74)90114-4
[30] Wilcox, D. C., "Formulation of the *k-w* Turbulence Model Revisited," AIAA, Paper 2007-1408, Jan. 2007.
[31] Wilcox, D. C., "Reassessment of the Scale-Determining Equation for Advanced Turbulence Models," *AIAA Journal*, Vol. 26, No. 11, 1988, pp. 1299–1310.
[32] Wilcox, D. C., *Turbulence Modeling for CFD*, DCW Industries, Inc., La Canada, CA, 1998.
[33] Smagorinsky, J., "General Circulation Experiments with the Primitive Equations," *Monthly Weather Review*, Vol. 91, 1963, pp. 99–164. doi:10.1175/1520-0493(1963)091<0099:GCEWTP>2.3.CO;2
[34] Strelets, M., "Detached Eddy Simulation of Massively Separated Flows," AIAA, Paper 2001-879, Jan. 2001.
[35] Bush, R. H., and Mani, M., "A Two-Equation Large Eddy Stress Model for High Sub-Grid Shear," AIAA, Paper 2001-2561, June 2001.
[36] Ni, R. H., "A Multiple Grid Scheme for Solving the Euler Equations," *AIAA Journal*, Vol. 20, 1982, pp. 1565–1571. doi:10.2514/3.51220
[37] Dannenhoffer, J. F., "Grid Adaptation for Complex Two-Dimensional Transonic Flows," Department of Aeronautics and Astronautics, Massachusetts Institute of Technology TR-87-10, Cambridge, MA, Aug. 1987.
[38] Davis, R. L., Ni, R. H., and Carter, J. E., "Cascade Viscous Flow Analysis Using the Navier–Stokes Equations," *Journal of Propulsion and Power*, Vol. 3, No. 5, Sept.–Oct. 1987.
[39] Davis, R. L., Hobbs, D. E., and Weingold, H. D., "Prediction of Compressor Cascade Performance Using a Navier–Stokes Technique," *Journal of Turbomachinery*, Vol. 110, No. 4, 1988, pp. 520–531. doi:10.1115/1.3262226
[40] Jameson, A., "Time Dependent Calculations Using Multi-Grid, with Applications to Unsteady Flows Past Airfoils and Wings," AIAA, Paper 91-1596, June 1991.
[41] Andrade, A. J., Davis, R. L., and Havstad, M. A., "A RANS/DES Numerical Procedure for Axisymmetric Flows with and Without Strong Rotation," AIAA, Paper 2008-702, Jan. 2008.
[42] Bozinoski, R., and Davis, R. L., "General Three-Dimensional Navier–Stokes Procedure for Reynolds-averaged and Detached-Eddy Simulations," AIAA, Paper 2008-756, Jan. 2008.
[43] Gropp, W., Lusk, E., and Skjellum, A., *Using MPI, Portable Parallel Programming with the Message-Passing Interface*, MIT Press, Cambridge, MA, 1999.
[44] Phillips, E. H., Zhang, Y., Davis, R. L., and Owens, J. D., "Rapid Aerodynamic Performance Prediction on a Cluster of Graphical Processing Units," AIAA, Paper 2009-565, Jan. 2009.
[45] Phillips, E. H., Davis, R. L., and Owens, J. D., "Unsteady Turbulent Simulations on a Cluster of Graphics Processors," AIAA, Paper 2010-5036, June 2010.
[46] Fife, M. E., and Davis, R. L., "A Conjugate Heat Transfer RANS/DES Simulation Procedure," AIAA, Paper 2009-913, Jan. 2009.
[47] Arts, T., Lambert de Rouvroit, M., and Rutherford, A. W., "Aero-Thermal Investigation of a Highly Loaded Transonic Linear Turbine Guide Vane Cascade," von Karman Institute for Fluid Dynamics, TN 174, Rhode-Saint-Genèse, Belgium, Sept. 1990.
[48] Mattingly, J. D., *Elements of Propulsion*, AIAA Education Series, AIAA, Reston, VA, 2006.
[49] Clark, J. P., Koch, P. J., Ooten, M. K., Johnson, J. J., Dagg, J., McQuilling, M. W., Huber, F., and Johnson, P. D., "Design of Turbine Components to Answer Research Questions in Unsteady Aerodynamics and Heat Transfer," U.S. Air Force Research Lab., Rept. AFRL-RZ-WP-TR-2009-2180, Wright-Patterson AFB, OH, Sept. 2009.

F. Liu
Associate Editor